energies

MDPI

Article

Assessment of Sensitivity to Evaluate the Impact of Operating Parameters on Stability and Performance in Proton Exchange Membrane Fuel Cells

Mingzhang Pan [1,2], Chengjie Pan [1], Jinyang Liao [1], Chao Li [1], Rong Huang [3] and Qiwei Wang [3,*]

[1] College of Mechanical Engineering, Guangxi University, Nanning 530004, China; pmz@gxu.edu.cn (M.P.); 1911301033@st.gxu.edu.cn (C.P.); 2011301029@st.gxu.edu.cn (J.L.); 1911392006@st.gxu.edu.cn (C.L.)
[2] Guangxi Key Laboratory of Electrochemical Energy Materials, Nanning 530004, China
[3] Postdoctoral Station of Mechanical Engineering, School of Automotive Studies, Tongji University, Shanghai 200092, China; lzwdycc@126.com
* Correspondence: 2190902174@cnu.edu.cn

Abstract: As a highly nonlinear system, the performance of proton exchange membrane fuel cell (PEMFC) is controlled by various parameters. If the effects of all parameters are considered during the performance optimization, low working efficiency and waste of resources will be caused. The development of sensitivity analysis for parameters can not only exclude the parameters which have slight effects on the system, but also provide the reasonable setting ranges of boundary values for simulation of performance optimization. Therefore, sensitivity analysis of parameters is considered as one of the methods to optimize the fuel cell performance. According to the actual operating conditions of PEMFC, the fluctuation ranges of seven sets of parameters affecting the output performance of PEMFC are determined, namely cell operating temperature, anode/cathode temperature, anode/cathode pressure, and anode/cathode mass flow rate. Then, the control variable method is used to qualitatively analyze the sensitivity of main parameters and combines with the Monte Carlo method to obtain the sensitivity indexes of the insensitive parameters under the specified current density. The results indicate that among these parameters, the working temperature of the fuel cell is the most sensitive to the output performance under all working conditions, whereas the inlet temperature is the least sensitive within the range of deviation. Moreover, the cloud maps of water content distribution under the fluctuation of three more sensitive parameters are compared; the results verify the simulated data and further reveal the reasons for performance changes. The workload of PEMFC performance optimization will be reduced based on the obtained results.

Keywords: proton exchange membrane fuel cell; sensitivity analysis; working parameters; performance fluctuation; Monte Carlo method

check for updates

Citation: Pan, M.; Pan, C.; Liao, J.; Li, C.; Huang, R.; Wang, Q. Assessment of Sensitivity to Evaluate the Impact of Operating Parameters on Stability and Performance in Proton Exchange Membrane Fuel Cells. *Energies* **2021**, *14*, 4069. https://doi.org/10.3390/en14144069

Academic Editor: Ivan Tolj

Received: 8 May 2021
Accepted: 24 June 2021
Published: 6 July 2021

Publisher's Note: MDPI stays neutral with regard to jurisdictional claims in published maps and institutional affiliations.

Copyright: © 2021 by the authors. Licensee MDPI, Basel, Switzerland. This article is an open access article distributed under the terms and conditions of the Creative Commons Attribution (CC BY) license (https://creativecommons.org/licenses/by/4.0/).

1. Introduction

Proton exchange membrane fuel cell (PEMFC) is a kind of device that converts chemical energy in hydrogen directly into electrical energy. Its working principle can be concluded as the oxidation–reduction reaction of hydrogen and oxygen to generate electrons, and the transmission of electrons to form current [1,2]. The rate and degree of this process determine the performance of PEMFC, while the process is controlled by the coupling of multiple parameters [3–5].

The research on the influencing factors of PEMFC performance has always been a hot spot [6–8]. Abdallah et al. [9] obtained the optimal design parameters of PEMFC, which enables the best performance by comparing the power density curves of 30 kinds of cross-sectional flow channels under the same conditions. Zhao et al. [10,11] focused on the structural parameters of pore structures in PEMFCs and how to impact the mass transport and performance of PEMFCs. In addition to the inherent design parameters of PEMFC, the

effect of the working conditions such as temperature and pressure on the performance of PEMFC also cannot be ignored [12,13]. In the research of [14–16], the influence of dozens of environmental parameters on the performance of PEMFC was analyzed. However, the above research did not fully study all the parameters that affect the performance of PEMFC. These parameters interact to jointly control the internal reaction of PEMFC, which makes the optimization of PEMFC performance very complicated and cumbersome.

It can be noted that there are orders of magnitude difference in the degree of influence of different parameters on the performance of PEMFC [17–19]. Ghasabehi et al. [20] compared the effects of different operating parameters on the output power of fuel cells, then found the most effective cathode stoichiometric factor. According to the explanation in [21], the study is called sensitivity analysis of parameters, which describes the impact of parameter deviations on performance fluctuations' amplitude. It is necessary to analyze the sensitivity of the control parameters before starting performance optimization, because not only can the insensitive parameters be excluded according to the order of sensitivity, but also the parameter setting range that can improve the performance can be found according to the changing trends of polarization curves, which ultimately reduce the optimization workload [22]. Sensitivity analysis includes local sensitivity analysis (LSA) and global sensitivity analysis (GSA). GSA examines the overall impact of changes in multiple parameters on the results of the model operation and analyzes the impact of each parameter and its interaction on the model results [23], while with LSA, the basic principle is the controlled variable method, that is, one of the parameters is considered as the object of analysis, whereas the others are considered as constants. Vetter et al. [24] used the GSA and LSA simultaneously to list the comprehensive ranking of model parameters, which can predict the behavior of the fuel cell under unknown conditions. When the parameters of sensitivity analysis are few, similar results can be obtained by these two analyzed methods. Compared with GSA, LSA requires less simulation. Therefore, LSA was employed in this study to analyze the sensitivity analysis of PEMFC parameters.

Before analyzing the sensitivities of parameters, it is necessary to combine and rank the analyzed parameters to choose the adequate fluctuated ranges of parameters. Jin et al. [25] used the Box–Behneken design (BBD) method to select the optimal combination conditions of parameters; however, it requires multiple simulations before sensitivity analysis. To save computational resources, the fluctuated ranges of working parameters are calibrated by experience. Local sensitivity analysis based on control variable method has been mentioned in many studies about sensitivity analysis [26–28]. Min et al. [29] considered 11 parameters, including porosity and diffusion coefficient, and classified these parameters according to the sensitivity indexes obtained by their corresponding polarization curves. Moreover, it can be found that parameters of the cathode side have a more sensitive effect on performance than the anode side. However, there is no specific analysis process in the literature, and these conclusions are only obtained by observing the changes of these polarization curves. This judgment method will cause errors, that is, the uncertainty mentioned in [30]. Therefore, sensitivity analysis and uncertainty analysis of parameters must usually be carried out synchronously. Sobol et al. [31] introduced the application of Monte Carlo method in sensitivity analysis of nonlinear mathematical model in detail. On the basics of the analysis method proposed by Zhao et al. [32], Monte Carlo method and the concept of sensitivity index [29] were introduced into the study, and then the sensitivity analysis of five design parameters and five performance parameters of PEMFC was carried out, so that the obtained conclusions could be supported by data. Nevertheless, it can be found in the study of Chen et al. [33] that when the current density increases from 200 A/cm^2 to 1200 A/cm^2, the output voltage, the average oxygen concentration, and the deviation of the oxygen concentration distribution are used as evaluation indicators to obtain completely different sensitivity rankings of parameters. Therefore, huge errors will be caused if the sensitivity of parameters is roughly divided according to only one current load mode. Focused on the shortcomings in previous workings, a three-dimensional, non-isothermal fuel cell model and some innovations are employed in this paper.

- To make the obtained sensitivity indexes comparable, this paper combined with the actual operating conditions to uniformly delineate the calibration parameters and their fluctuation ranges before starting the sensitivity analysis. Moreover, a reliable parameter sensitivity assessment method was designed.
- The Monte Carlo method was adopted to quantitatively analyze the parameters, which have little effect on the output performance (failed to judge by the deviation percentages) under calibration conditions. The parameter sensitivity rankings under specific current density were obtained.
- In addition to determining the impact of single parameter fluctuations on the output voltage, the water content distribution cloud maps of the contact surface between anode side catalyst layer (CL) and membrane are used to prove the improvement/deterioration of PEMFC performance, which can intuitively explain the phenomena.

Finally, according to the sensitivity indexes, the parameters were classified as insensitive, sensitive, and highly sensitive. The results provide a reference for the optimization of PEMFC and the controls of operating parameters.

2. Description of Model

2.1. Governing Equation

In [34], the equations of conservation of mass, momentum, energy, species, and charges were summarized into a general convection–diffusion equation, as follows:

$$\nabla\cdot(\rho v\phi) = \nabla\cdot(\Gamma_\phi \nabla_\phi) + S_\phi \tag{1}$$

However, this equation is applicable in the steady state. In this study, an unsteady state model was constructed. Thus, a new general governing equation may be formulated, as follows:

$$\frac{\partial(\rho\phi)}{\partial t} + \nabla\cdot(\rho v\phi) = -\nabla p + \nabla\cdot(\Gamma_\phi \nabla_\phi) + S_\phi \tag{2}$$

where ρ and p refer to nominal density and pressure, respectively, ϕ is a general variable and the velocity vector is represented by v. The symbols p, ϕ, ρ, and Γ_ϕ for various equations are listed in Table 1.

Table 1. ρ, ϕ, Γ_ϕ of different governing equations.

	Mass	Momentum	Energy	Species	Charges
ϕ	1	v	T	εY_i	ϕ_s, ϕ_mem
ρ	ρ_mix	ρ_mix	$\rho_\mathrm{mix}C_\mathrm{p}$	ρ_mix	0
Γ_ϕ	0	μ_eff	λ_eff	$\rho_\mathrm{mix}D_\mathrm{i}^\mathrm{eff}$	σ_s, σ_mem
p	0	p_liq	0	0	0

2.2. Electrochemical Reaction Model

After describing the phenomena of mass transfer, heat transfer, and electricity transfer in PEMFC using the governing conservation equation, the electrochemical reaction model of the cathode catalyst layer was constructed. According to Dickinson et al. [35], most PEMFC models use the Butler–Volmer equation to describe the electrode kinetics:

$$i = \mathrm{i}_0\left(\exp\left(\frac{\alpha_\mathrm{Rd}\mathrm{F}(E-E_\mathrm{r})}{\mathrm{R}T}\right) - \exp\left(-\frac{\alpha_\mathrm{Ox}\mathrm{F}(E-E_\mathrm{r})}{\mathrm{R}T}\right)\right) \tag{3}$$

where α_Rd and α_Ox represent the transfer coefficients of the reduction and oxidation reactions, respectively. F, T and R represent the Faraday, temperature, and gas constants, respectively. E denotes the electrode potential and E_r refers to the equilibrium potential; the difference between them is referred to as the overpotential, which is usually represented by η, see Equations (4) and (5).

$$\eta_\mathrm{an} = E_\mathrm{a} - E_\mathrm{r,a} \tag{4}$$

$$\eta_{\mathrm{ca}} = E_{\mathrm{c}} - E_{\mathrm{r,c}} \tag{5}$$

The overpotential of the anode is positive, which refers to electrons moving away from the electrode. Similarly, the value obtained from Equation (5) is negative. For the anode and cathode reactions to occur in the fuel cell, the Butler–Volmer equation is also effective:

$$R_{\mathrm{an}} = (\xi_{\mathrm{an}} j_{\mathrm{an}}(T)) \left(\frac{[A]}{[A]_{\mathrm{ref}}} \right)^{\gamma_{\mathrm{an}}} \left(\exp\left(-\frac{\alpha_{\mathrm{Rd}}^{\mathrm{an}} \mathrm{F} \eta_{\mathrm{an}}}{\mathrm{R}T} \right) - \exp\left(\frac{\alpha_{\mathrm{Ox}}^{\mathrm{an}} \mathrm{F} \eta_{\mathrm{an}}}{\mathrm{R}T} \right) \right) \tag{6}$$

$$R_{\mathrm{an}} = (\xi_{\mathrm{an}} j_{\mathrm{an}}(T)) \left(\frac{[A]}{[A]_{\mathrm{ref}}} \right)^{\gamma_{\mathrm{an}}} \left(\exp\left(-\frac{\alpha_{\mathrm{Rd}}^{\mathrm{an}} \mathrm{F} \eta_{\mathrm{an}}}{\mathrm{R}T} \right) - \exp\left(\frac{\alpha_{\mathrm{Ox}}^{\mathrm{an}} \mathrm{F} \eta_{\mathrm{an}}}{\mathrm{R}T} \right) \right) \tag{7}$$

where $j(T)$ is the reference exchange current density per effective surface area ($\mathrm{A/m^2}$), ξ is the activation area ratio (1/m), $\frac{[A]}{[A]_{\mathrm{ref}}}$ and $\frac{[C]}{[C]_{\mathrm{ref}}}$ represent the ratio of the local component concentration to the reference value in the anode and cathode, respectively, γ refers to the concentration index, $\alpha_{\mathrm{Rd}}^{\mathrm{an}}$ and $\alpha_{\mathrm{Rd}}^{\mathrm{cat}}$ are the anode and cathode charge transfer coefficients of the reduction reaction, respectively, $\alpha_{\mathrm{Ox}}^{\mathrm{an}}$ and $\alpha_{\mathrm{Ox}}^{\mathrm{cat}}$ express the anode and cathode charge transfer coefficients of the oxidation reaction.

2.3. Membrane Electrode Water Transport Model

The following transport equation describes the membrane electrode liquid water saturation:

$$\begin{aligned} \frac{\partial(\varepsilon \rho_{\mathrm{l}} \mathrm{S})}{\partial t} + \nabla \cdot \quad & \left(\varepsilon \rho \nu \lambda_{\mathrm{l}} + \frac{\alpha M_{\mathrm{l}}}{\mathrm{F}} i_{\mathrm{e}} \right) \\ & = \nabla \cdot (\varepsilon \rho_{\mathrm{l}} D_{\mathrm{c}} \nabla \mathrm{S}) - \nabla \cdot \left(\frac{\lambda_{\mathrm{l}} (1 - \lambda_{\mathrm{l}}) \mathrm{k} \left(\rho_{\mathrm{l}} - \rho_{\mathrm{g}} \right)}{v} \right) + S_{\mathrm{l}} \end{aligned} \tag{8}$$

where S is the liquid water saturation, which characterizes the ratio of the volume occupied by the liquid water to the volume of the void in the porous medium of the membrane electrode. λ_{l}, M_{l}, i_{e}, ρ_{l}, and ρ_{g}, refer to the relative mobility of liquid water, the molar mass of liquid water, electrolyte phase current density, liquid water density, and gaseous water density, respectively. D_{c} is the capillary diffusion coefficient of liquid water and is defined by the following Equation:

$$D_{\mathrm{c}} = -\left(\frac{k_{\mathrm{l}}}{\mu_{\mathrm{l}}} \right) \frac{dp_{\mathrm{c}}}{ds} \tag{9}$$

In this equation, k_{l}, p_{c}, μ_{l}, and S_{l} represent the liquid water permeability, capillary pressure, dynamic viscosity of liquid water, and source term of water phase transition, respectively; S_{l} is defined as

$$S_{\mathrm{l}} = \begin{cases} M_{\mathrm{l}} k_{\mathrm{cond}} \frac{(\varepsilon X_{\mathrm{w}})}{\mathrm{R}T} (X_{\mathrm{w}} p - p_{\mathrm{sat}}) & (X_{\mathrm{w}} p > p_{\mathrm{sat}}) \\ M_{\mathrm{l}} k_{\mathrm{evap}} \frac{(\varepsilon \mathrm{S} \rho_{\mathrm{l}})}{\mathrm{R}T} (X_{\mathrm{w}} p - p_{\mathrm{sat}}) & (X_{\mathrm{w}} p \leq p_{\mathrm{sat}}) \end{cases} \tag{10}$$

where X_{w} represents the mass fraction of water vapor on the proton membrane surface and k_{cond} and k_{evap} are the condensation of water and evaporation rate coefficients, respectively. The latent heat of phase transition in water is expressed as

$$S_{\mathrm{h}} = m_{\mathrm{l}} h_{\mathrm{c}} \tag{11}$$

where h_{c} is the latent heat of phase transition in water.

The water content in the membrane is maintained in a dynamic equilibrium state, which is essential for managing the water content in the fuel cell under working conditions. When the cell is working, the water content in the membrane is determined using water transport by the membrane. Water can be transported in four ways in a proton membrane: through ionic conduction, electroosmotic drag, back-diffusion, and hydraulic permeability.

As one of the most significant parameters within the PEM, the proton conductivity is always represented by the symbol σ (S/cm), which is used to evaluate the transport capacity of the protons. The proton conductivity of the PEM materials with resistance can be expressed as

$$\sigma = \frac{I}{(R_s S)} \tag{12}$$

where R_S refers to the overall impedance of the membrane samples, I is the distance between the reference electrodes, and S is the cross-sectional area of the membrane samples.

Electroosmotic drag is caused by the anode side of the polar water molecules and proton hydration, and ($H^+(nH_2O)$) is formed. The water molecules migrate from the anode to the cathode side with protons, and the corresponding water migration flux caused by the electroosmotic dragging of the proton membrane can be expressed as

$$N_{eod} = n_d(\lambda)\frac{i}{F} \tag{13}$$

where i and λ are the current density and water content of the membrane, respectively. $n_d(\lambda)$ is the electroosmotic drag coefficient, which represents the number of water molecules carried by each proton (dragged) transported. $n_d(\lambda)$ is a function of the proton membrane water content (λ) and can be expressed by the following widely used empirical expression:

$$n_d(\lambda) = 2.5 \times \frac{\lambda}{22} \tag{14}$$

The reverse diffusion water transfer flux is related to the water concentration gradient on both sides of the proton membrane [36,37]:

$$N_{bd} = -\frac{\rho_m}{EW} D_m \frac{\partial c}{\partial y} \tag{15}$$

where D_m represents the diffusion coefficient of water molecules in the membrane and $\frac{\partial c}{\partial y}$ is the water concentration gradient, which is distributed on both sides of the proton membrane.

As one of the water transport methods within the membrane, hydraulic permeability is caused by the pressure difference between the anode and cathode. Compared to other transport mechanisms, the amount of water transferred through hydraulic permeability is at least one order of magnitude lower [38]. Therefore, the impact of this parameter is ignored in this paper. The source terms of various governing equations are listed in Table 2.

Table 2. Source terms of governing equations.

Computational Domain	Source Term					
	Mass S_m	Momentum S_u	Energy S_T	Species S_i	Potential S_{ele}	Potential S_{ion}
Bipolar plate	0	0	$\|\nabla\varphi_{ele}\|^2 k_{ele}^{eff}$	0	0	0
Flow channel	0	0	0	0	0	0
Gas diffusive layer	0	$-\frac{\mu_{eff}}{k}\varepsilon^2 v$	$\|\nabla\varphi_{ele}\|^2 k_{ele}^{eff} + m_i h_c$	0	0	0
Anode catalyst layer	$-\frac{R_a}{(2F)} M_{H_2}$	$-\frac{\mu_{eff}}{k}\varepsilon^2 v$	$j_a\|\eta_{act}\| + \|\nabla\varphi_{ele}\|^2 k_{ele}^{eff} + m_i h_c$	$\rho D_{i,eff}\frac{(Y_i - Y_{p,i})}{\delta}\left(\frac{S}{V}\right)_{eff}$	R_a	$-R_a$
Cathode catalystlayer	$\frac{R_c}{(4F)} M_{O_2} + \frac{R_c}{(2F)} M_{H_2O}$	$-\frac{\mu_{eff}}{k}\varepsilon^2 v$	$-\frac{(j_c T\Delta S)}{4F} + j_c\|\eta_{act}\| + \|\nabla\varphi_{ele}\|^2 k_{ele}^{eff} + m_i h_c$	$\rho D_{i,eff}\frac{(Y_i - Y_{p,i})}{\delta}\left(\frac{S}{V}\right)_{eff}$	$-R_c$	R_c
Proton exchangemembrane	0	0	$\|\nabla\varphi_{ion}\|^2 k_{ion}^{eff} + m_i h_c$	0	0	0

2.4. Boundary Conditions and Material Properties

The Dirichlet boundary condition was applied in this simulation.

(1) Anode/cathode adopted mass flow inlet (AMFR/CMFR): $C_a = C_{a,in}$ was used to define the mass fraction of each component of the reaction gas at the inlet.
(2) Channel outlet employed pressure outlet: $P = P_{an,out}$, $P = P_{ca,out}$ was used to define the anode and cathode pressures, respectively. Moreover, anode operating pressure (AOP) and cathode operating pressure (COP) are usually controlled by back pressure of PEMFC.
(3) The voltage or current density of the fuel cell model was set at the bipolar plate surface; the potential on the surface of the end plate of the anode and cathode bipolar plates can be expressed as $\phi_{ele}^{an} = 0$, $\phi_{ele}^{ca} = V_{cell}$.
(4) The no-slip wall boundary was applied to the wall interface between the fluid and solid computing domains.
(5) The operating temperature (COT) is expressed by the wall temperature of PEMFC [9,39], which can be independent of the anode inlet temperature (AIT) and cathode inlet temperature (CIT).

Properties of reactants:

(1) Stoichiometric ratio of hydrogen to air (excess coefficient):

In a fuel cell that uses high-purity hydrogen (99.999%) as fuel and air as oxidant, the excess coefficient of the anode can be expressed as

$$\psi_{an} = \frac{m_{H_2}^{in}}{\dot{m_{H_2}}} \tag{16}$$

where $m_{H_2}^{in}$ is the actual flow supplied by the anode hydrogen and $\dot{m_{H_2}}$ represents the theoretical demand flow when the target refers to the current density.

Similarly, the cathode excess coefficient can be expressed as

$$\psi_{ca} = \frac{m_{ca}^{in} \cdot y_{O_2}^{in}}{\frac{M_{O_2}}{4F} j_{ref} A_{act}} \tag{17}$$

(2) Relative humidity:

To decrease the ohmic resistance, humidifying the reactant gas is necessary. The relative humidity (*RH*) is usually used to characterize the degree of inlet humidity and can be defined as

$$RH = \frac{P_{sat}^{in}}{[P_{sat}(T)]} \times 100\% \tag{18}$$

where P_{sat}^{in} refers to the saturated vapor pressure corresponding to the humidification temperature of the gas inlet and $P_{sat}(T)$ is the saturated vapor pressure corresponding to the operating temperature of cell.

2.5. Geometric Model and Meshing

At least nine computational fields exist in a three-dimensional model of a complete PEMFC—bipolar plates sites in the cathode and anode, respectively, cathode/anode flow channels, cathode/anode gas diffusive layers (GDL), cathode/anode catalyst layers (CL), and the proton exchange membrane (PEM). Owing to the feature of parallel channel symmetry, to reduce the amount of calculation, half of a complete PEMFC model with a single straight flow channel was truncated along the symmetric plane. A 3D model design software known as UG (Unigraphics NX, developed by Siemens) was used in this study, and the computational domain model covered all directions. In this study, the grid division strategy of a regular hexahedral structure was adopted; compared to unstructured grids

such as tetrahedral prisms, it calculates quickly, converges easily, and controls the grid nodes conveniently.

Meshing in ICEM is depicted in Figure 1a. Four sets of regular hexahedral structural grids were prepared with the number of grid elements 100,468, 128,600, 140,400, 158,400 to validate the grid independence. The current density under the given working voltage can comprehensively reflect the degree of electrochemical reaction inside the cell, the multicomponent transportation of the reaction gas, and the performance of charge travel. Thus, this study validated the grid independence with the current density corresponding to the operating voltage of 0.7 V under certain working conditions, which set the intake and exhaust pressures of the cathode/anode as 2 atm, operating temperature as 80 °C, and humidity as 100%, as depicted in Figure 1b. The current density corresponding to the number of grid elements, 100,468, was approximately 0.386 A/cm^2; the number of grid elements should be avoided because of its larger deviation compared to other grids. Comprehensively considering the computational stability and efficiency, the number of grid elements of 140,400 was eventually elected as the calculated number of grid elements. The details of the configuration are presented in Table 3.

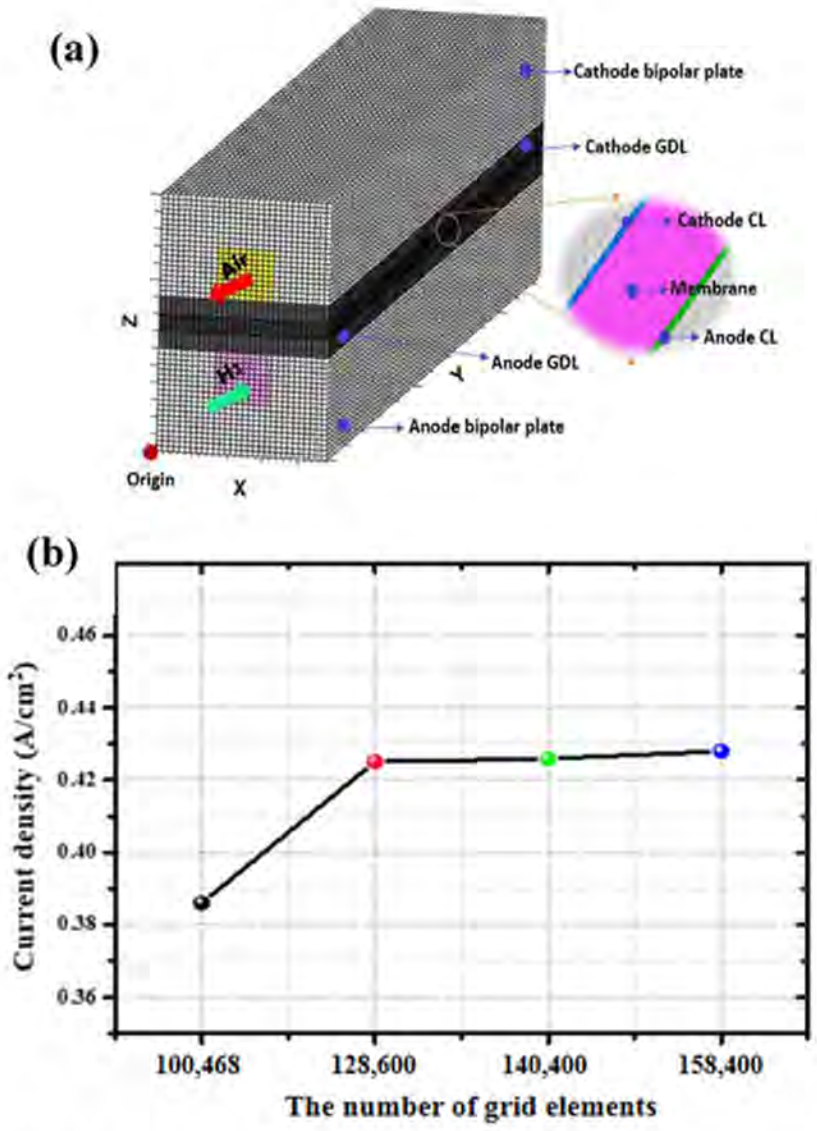

Figure 1. Grid related: (**a**) meshing of computational domain, (**b**) validation of grid independence.

Table 3. Geometry parameters of PEMFC and the number of grid elements (NGE).

Compute Domain Name	X(mm)/NGE	Y(mm)/NGE	Z(mm)/NGE
45,000 Bipolar plate	2.4/25	100/60	2/15
8400 Flow channel	0.8/10	100/60	0.8/7
30,000 Gas diffusive layer	2.4/25	100/60	0.25/10
15,000 Catalyst layer	2.4/25	100/60	0.014/3
42,000 Proton exchange membrane	2.4/25	100/60	0.23/14

3. Results and Discussion

3.1. Model Validation

A variety of phenomena that can be expressed by the polarization curve, such as convection and diffusion transport performance of reactive gas in PEMFC, charge transfer resistance in the membrane and solid phases, as well as the state of electrochemical reaction, have a comprehensive impact on cell performance. Therefore, it is usual to contrast the tendency of the polarization curve in simulation with that in the experiment.

In this paper, the working parameter was set the same as that in [9]; thereafter, the numerical simulation was started. The simulated results of this paper are compared with the simulated results obtained by Mohammedi et al., as can be seen in Figure 2. The numerical results are basically consistent with the polarization curve and power density curve in literature; compared with the middle-current-density region, the numerical agreement is better in the high- and low-current-density region. There are the larger differences in the ohmic region, which means more serious ohmic polarization loss in the simulated model of this paper. The main reason is that some physical properties of PEMFC are not provided in the reference, especially the electronic conductivity, ionic conductivity, and anode/cathode reference concentration. According to the literature [40,41], the ionic conductivity has remarkable effects on the resistance of PEMFC. Moreover, the reference concentration of anode and cathode and the permeability coefficient and viscosity of the mixed gas all have effects on the output performance of PEMFC. However, the error is within an acceptable range, which can be used to predict the performance.

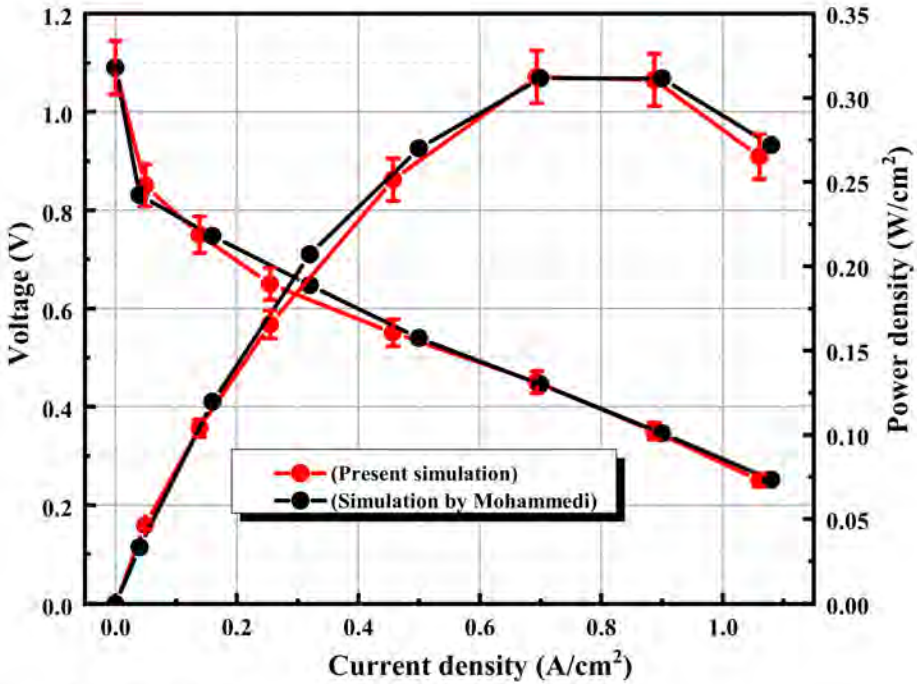

Figure 2. Model validation.

3.2. Parameter Setting

The Monte Carlo method with multiparameter sensitivity analysis was used in this part of the experiment, under the common calibration condition of vehicle-used PEMFC, which is aimed at quantitatively analyzing the impact of fluctuating parameters (±5%) on the sensitivity of output performance.

The common calibration conditions used in cars include the idle condition and rated condition. The idle condition means starting the fuel cell engine but not driving the car. At this time, the energy provided by the fuel cell system is required only to maintain the normal working of the subsidiary parts.

In this part, two types of working conditions are used as inlet conditions in the single cell. Under a state of low power, the output current density of the cell is approximately 0.1 A/cm^2. The rated condition means that the cell is running at the rated output power and the output current density is approximately 0.6 A/cm^2. A current density of 0.3 A/cm^2 is chosen as the intermediate working condition. Table 4 lists the calibration parameters and their range of fluctuation. Table 5 provides the inlet boundary conditions.

Table 4. Calibration parameters and the fluctuation ranges.

Operating Parameters	Symbol	Calibration Value (Unit)	Range
COT	T_{cell}	70 (°C)	66.5 ~ 73.5 (±5%)
AOP	P_{an}	1 (atm)	0.95 ~ 1.5(±5%)
COP	P_{ca}	1 (atm)	0.95 ~ 1.5 (±5%)
AIT	T_{an}	70 (°C)	66.5 ~ 73.5(±5%)
CIT	T_{ca}	70 (°C)	66.5 ~ 73.5 (±5%)
AMFR	$m^{in}_{H_2}$	6×10^{-7} (kg/s)	5.7×10^{-7} ~ 6.3×10^{-7} (±5%)
CMFR	m^{in}_{ca}	5×10^{-6} (kg/s)	4.75×10^{-6} ~ 5.25×10^{-6} (±5%)

Table 5. Boundary conditions and material properties [9,37].

Parameters	Value	Unit	Parameters	Value	Unit
Open circuit voltage (E)	1.09	V	CL viscous resistance (μ^{eff}_{CL})	1.76×10^{11}	1/m^2
Anode reference current density (j_{an}(T))	71.7	A/m^2	Anode/cathode CL surface to volume ratio (ξ_{an}/ξ_{ca})	1.127×10^7	1/m
Cathode reference current density (j_{ca}(T))	7.17×10^{-4}	A/m^2	Membrane equivalent weight (EW)	1100	kg/kmol
Anode/cathode reference concentration ($[A]_{ref}/[C]_{ref}$)	1	kmol/m^3	GDL viscous resistance (μ^{eff}_{GDL})	1.76×10^{11}	1/m^2
Anode concentration exponent (Γ_{an})	0.5	-	Membrane density (ρ_m)	1980	kg/m^3
Cathode concentration exponent (Γ_{ca})	1	-	Ionic conductivity (σ_{mem})	9	S/m
Anode/cathode exchange coefficient of reduction reaction ($\alpha^{an}_{Rd}/\alpha^{cat}_{Rd}$)	1.5	-	Electrical conductivity (σ_s)	1000	S/m
Anode/cathode exchange coefficient of oxidation reaction ($\alpha^{an}_{Ox}/\alpha^{cat}_{Ox}$)	2	-	Specific heat capacity of the membrane; CL; GDL; BP; H_2; O_2 (C_p)	833; 3300; 568; 871; 14,283; 919	J/(kg•K)
H_2 diffusivity ($D^{eff}_{H_2}$)	2.25×10^{-5}	m^2/s			
O_2 diffusivity ($D^{eff}_{O_2}$)	1.13×10^{-5}	m^2/s			
H_2O diffusivity ($D^{eff}_{H_2O}$)	1.35×10^{-5}	m^2/s	CL porosity (ε_{CL})	0.4	
Relative humidity (RH)	100%		GDL porosity (ε_{GDL})	0.6	

The impact of fluctuation of the operating parameters (the corresponding current densities are 0.1 A/cm^2, 0.3 A/cm^2, and 0.6 A/cm^2) within a certain range on the cell

output voltage under common operating conditions of automobiles is studied in this paper and the results can be seen in Section 3.3. The calibration parameters and their fluctuation ranges are displayed in Table 4. Under these conditions, the behavior of ΔV, which represents the deviation of the PEMFC output voltage as well as the percentage change in voltage deviation, was investigated. The percentage change in the voltage deviation is defined as $|(\Delta V)/V| \times 100\%$, where V is the calibration condition voltage and $\Delta V = V_{\text{test}} - V$.

3.3. Simulation Results

The pictures of polarization curves and voltage deviations are presented in different parts of Section 3.3 to analyze the effect of different parameters and their deviations on performance.

3.3.1. Deviation of Cell Operating Temperature

Figure 3 depicts how the deviation of cell operating temperature (COT) impacts the deviation of the output voltage and the percentage of deviation when other calibration parameters are maintained constant. The relationship between the cell operating temperature and voltage is negative correlation, which means that at the same current density, the deviation of voltage is negative and larger as the current density increases (see Figure 3a). The main reason is that when other parameters are kept constant, the lifting COT increases the saturated vapor pressure of water. The relative humidity (RH) of the reactant gas decreases, which weakens the hydration of the proton membrane, reduces the water content in the membrane, increases the ohmic resistance, and lowers the output voltage. Moreover, under the same deviation of temperature, as the current increases, increasingly more water is produced, which increases the ohmic losses. Therefore, the value of the amplitude of negative deviation at 0.6 A/cm^2 is the largest.

To quantify the effect of OCT fluctuation on the output voltage under three values of current density (0.1 A/cm^2, 0.3 A/cm^2, 0.6 A/cm^2) in Figure 3a, Figure 3b shows the voltage deviations (ΔV) and their deviation percentages corresponding to the temperature deviations. It can be seen that the overall amplitude of fluctuation is smooth when the current density is 0.1 A/cm^2. This is because when the current density is low, there is less water produced by electrochemical reaction and less water accumulated in the porous media layer, which will cause a decrease in the amplitude of performance changes. The lifting and declining amplitudes of the voltage are low compare with high current density.

3.3.2. Deviation of Cathode Operating Pressure

Figure 4 shows the impact of deviation of the cathode operating pressure (COP) on the deviation of the output voltage and the deviation percentage under various current densities. This is in agreement with the upper segment results. COP is positively correlated with the fuel cell output voltage at the same current density, that is, the voltage deviation is positive and increases the same as the increase of the COP at the same current density (see as Figure 4a). According to the data in Figure 4b, the change trend of output voltage with cathode pressure under three current densities is similar under three kinds of current density and the amplitudes of deviation under different cathode pressure increase with the increase of current density. The magnitude of deviation/percentage in Figure 4b indicates that the impact of cathode pressure fluctuation on PEMFC performance is second only to COT.

The main reason for this phenomenon may be due to the supplied gas for the cathode inlet being air (oxygen only accounts for 21%). The fluctuated operating cathode pressure has a great influence on the oxygen concentration in cathode CL, which in turn affects the performance of PEMFC. As for why there are obvious differences of polarization curves among five kinds of COP at high current density, it may be explained that changing the pressure can change the limiting current density, which means that only the high current density (the region close to the limiting current density) can be significantly influenced.

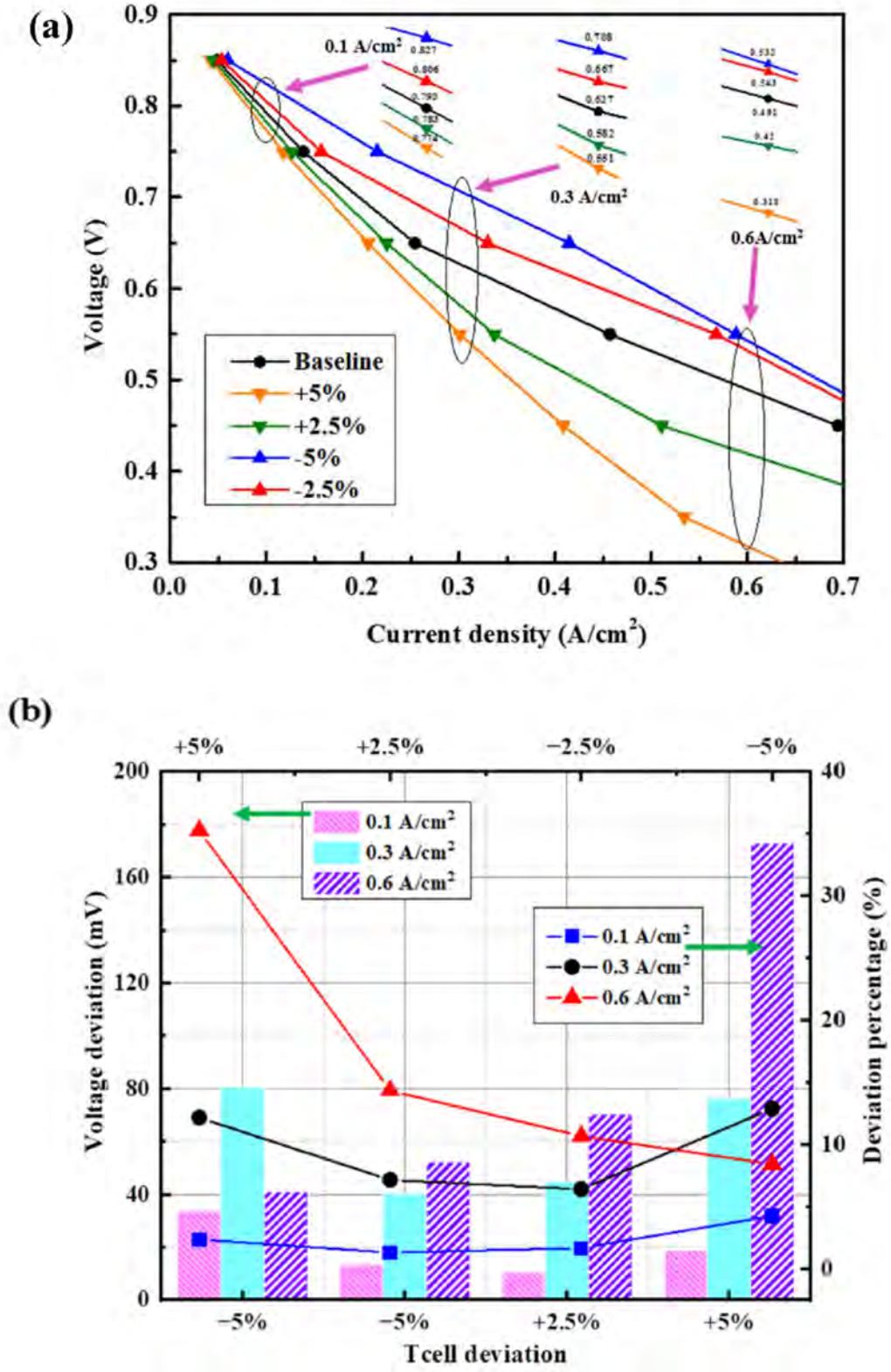

Figure 3. Impact of COT deviation on voltage: (**a**) polarization curves of different cell temperature, (**b**) the voltage deviation obtained by COT deviations and their corresponding percentages under three current densities. −5%.

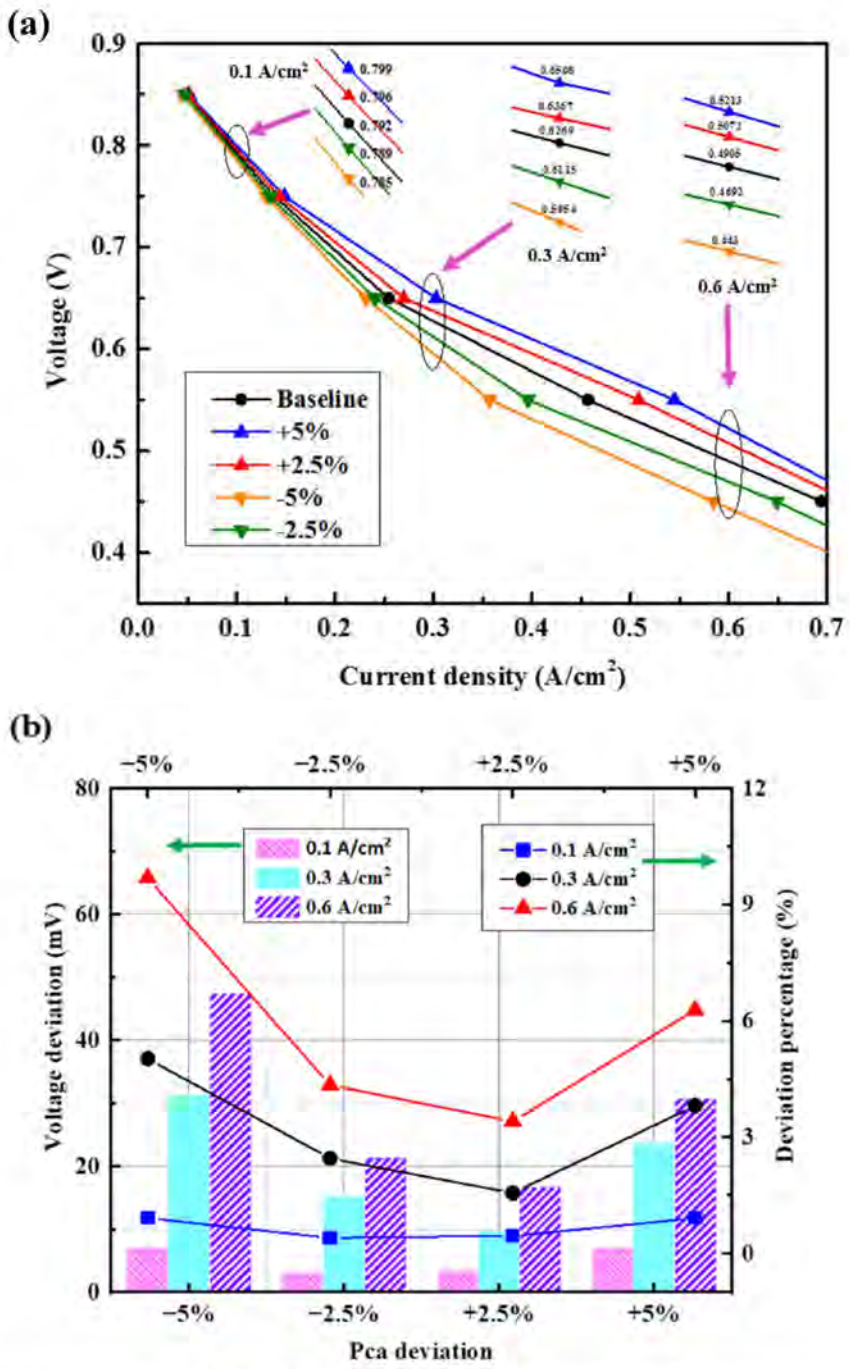

Figure 4. Impact of COP deviation on voltage: (**a**) polarization curves of different cathode operating pressure, (**b**) the voltage deviation obtained by COP deviations and their corresponding percentages under three current densities.

3.3.3. Deviation of Anode Pressure

The impact of deviation of the anode operating pressure (AOP) on the polarization curves and the output deviation/deviation percentage depicted in Figure 5a is lower compared with Figure 5b. However, the fluctuating trends of the output voltage and the corresponding percentages shown in Figure 5b are basically the same as that in Figure 5a. Same as the theory of air transfer in the cathode, the increase in anode pressure promotes the convection diffusion of hydrogen molecules in the porous layer of the anode, which enhances the mass transfer performance of hydrogen, increases the exchange current density, and reduces the loss of concentration, finally improving the performance of the

fuel cell. Meanwhile, the oxygen required in the cathode will increase to participate in the reaction with hydrogen in time. However, the increase of anode pressure will prevent the oxygen mass transfer in the cathode side, that is, the oxidation–reduction reaction will be hindered. Therefore, the influence of AOP fluctuation on the output voltage is inferior to the fluctuation of COP.

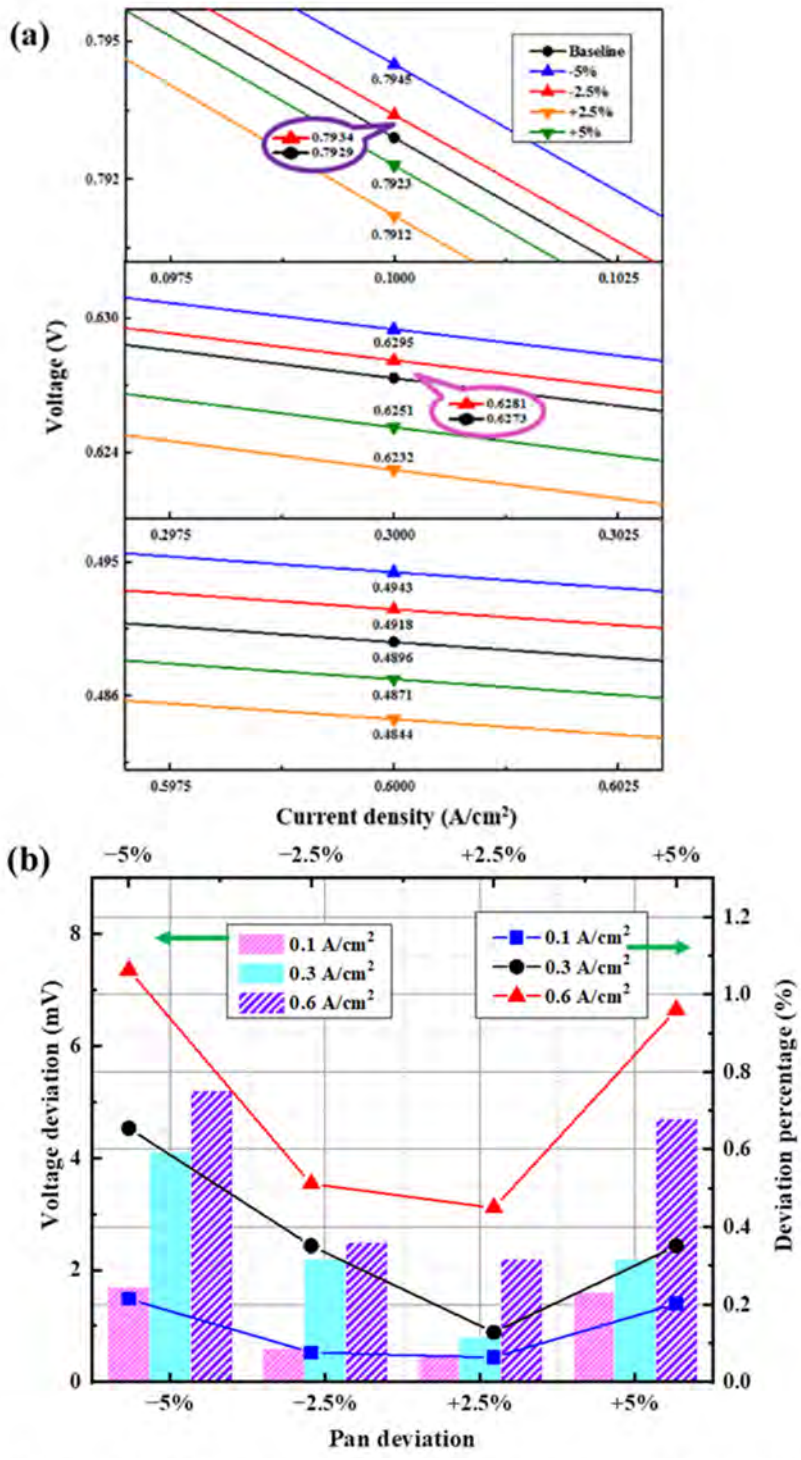

Figure 5. Impact of AOP deviation on voltage: (**a**) polarization curves of different anode operating pressure, (**b**) the voltage deviation obtained by AOP deviations and their corresponding percentages under three current densities.

3.3.4. Deviation of Anode Mass Flow Rate

Figure 6 depicts when the calibration intake parameters are maintained constant, how the deflection in the anode mass flow rate (AMFR) impacts the deviation of the output voltage, and the percentage of deviation under various current densities. Figure 6a,c indicates that the relationship between the AMFR and the cell performance is a negative correlation, that is, at the same current density, the cell output voltage decreases as a function of the deviation of the AMFR. Meanwhile, the amplitude of the voltage deviation increases with an increase in the deviation of the AMFR.

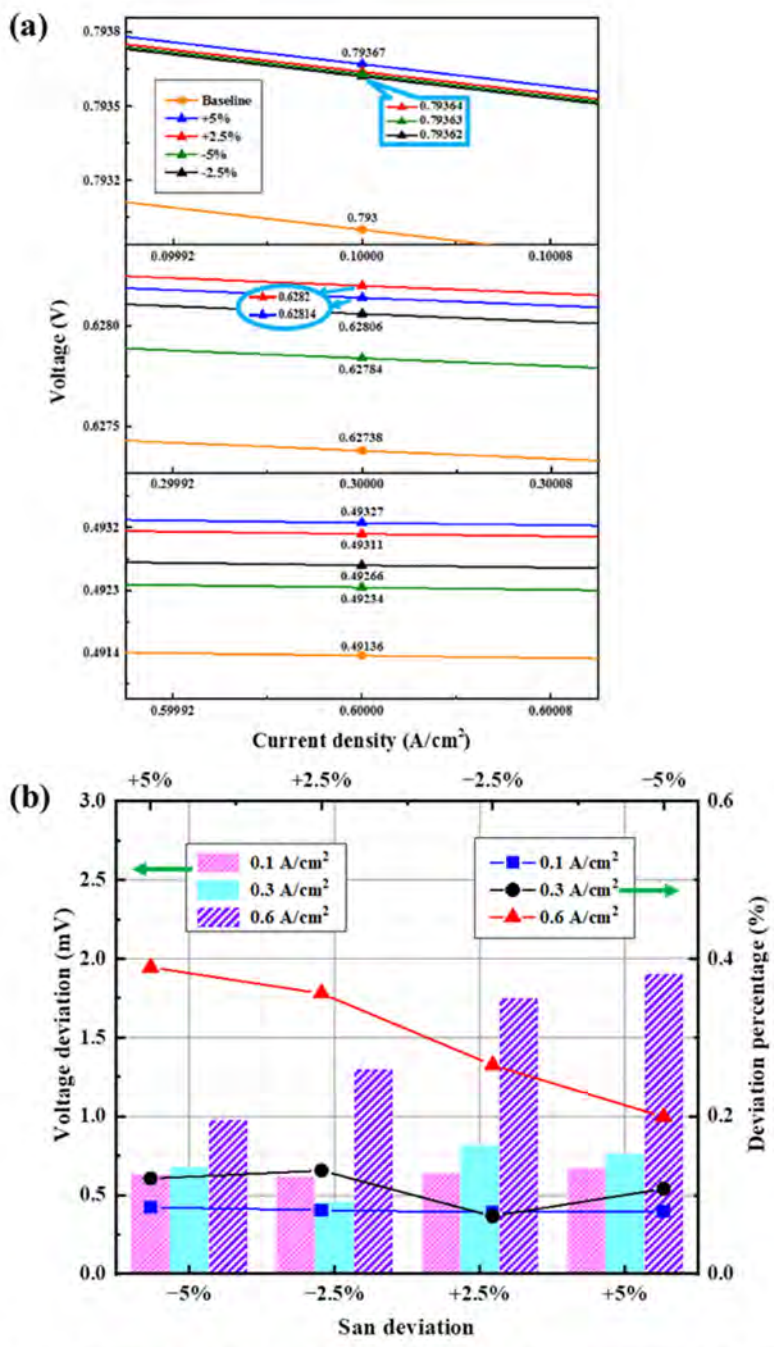

Figure 6. Impact of AMFR deviation on voltage: (**a**) polarization curves of different anode mass flow rate, (**b**) the voltage deviation obtained by AMFR deviations and their corresponding percentages under three current densities.

To explore the reason for the large changes in output voltage in Figure 7 when the current density is high, the cloud maps of water content distribution in the contact region between the anode CL and GDL when the fluctuations of AMFR are ±2.5%, ±5%, respectively, and current density is 0.6 A/cm^2 are shown in Figure 7. Although there is a minimal current density that occurs when the AMFR is 6×10^{-7} kg/s, the overall distribution of water content within the interface seems to more evenly compared with the values of AMFR, which are 5.85×10^{-7} kg/s and 5.7×10^{-7} kg/s, respectively. Especially when the mass flow rate is 5.7×10^{-7} kg/s, large areas of extreme water content are distributed in different areas of the interface. With the AMFR increasing, high water content areas occur accompanied with the increase of water content in the central areas of the interface. The anode is drier than the cathode due to redox reaction; the excessive low water content in anode will decrease the performance of PEMFC, so the performance of PEMFC can be improved by enhancing the anode water content.

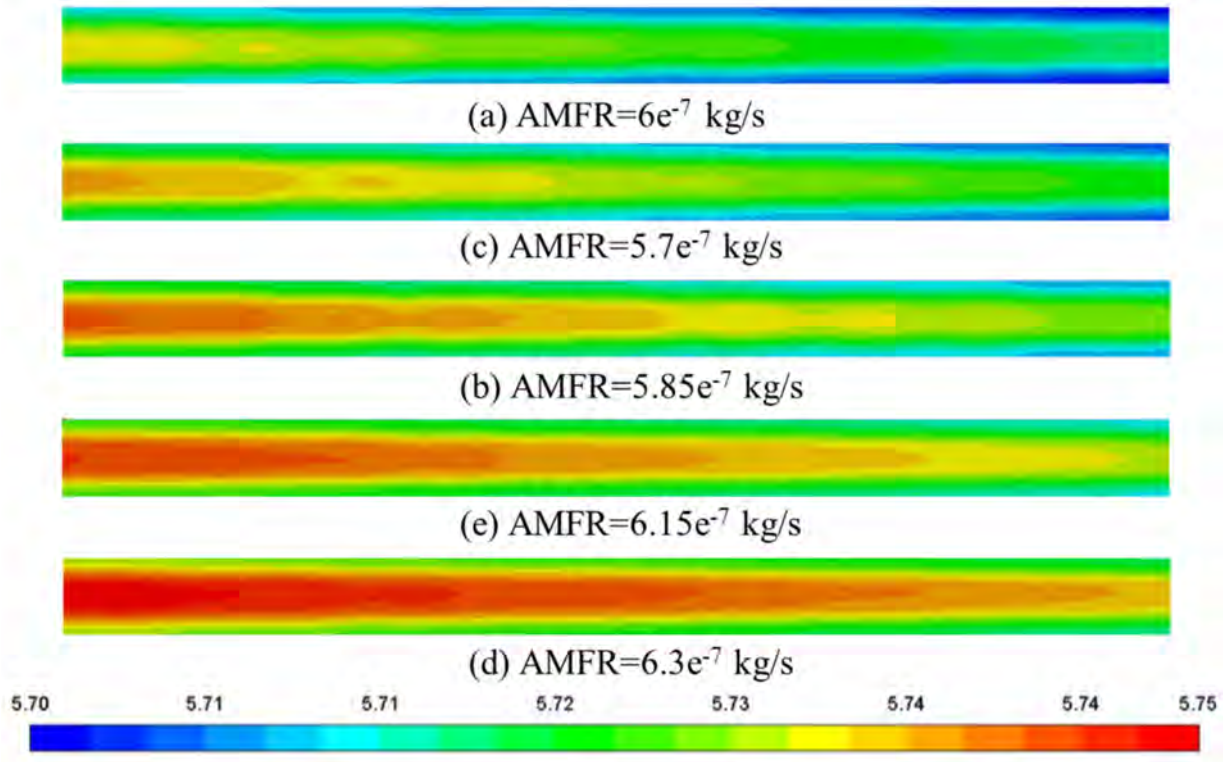

Figure 7. Water content distribution under the fluctuation of AMFR.

3.3.5. Deviation of Cathode Mass Flow Rate

The effects of the fluctuations of cathode mass flow rate (CMFR) on the polarization curves are too small to be observed clearly. Comparing both sides of the *y*-axis in Figures 6b and 8, it can be found that the influence of the fluctuated CMFR on the output voltage is in the same order of magnitude as that of fluctuated AMFR. Moreover, the deviations caused by the fluctuated CMFR are not affected by current density, especially when the load current is relatively large. On the one hand, the improvement of air flow rate bonds to increase the oxygen concentration in CL, which will promote the redox reactions in three-phase areas. On the other hand, with the flow rate increasing, the water removal rate of the cathode side increases. Finally, the performance of PEMFC is reduced because of the dehydration of membrane. Therefore, the trend of the output voltage deviation depends on the dominant party.

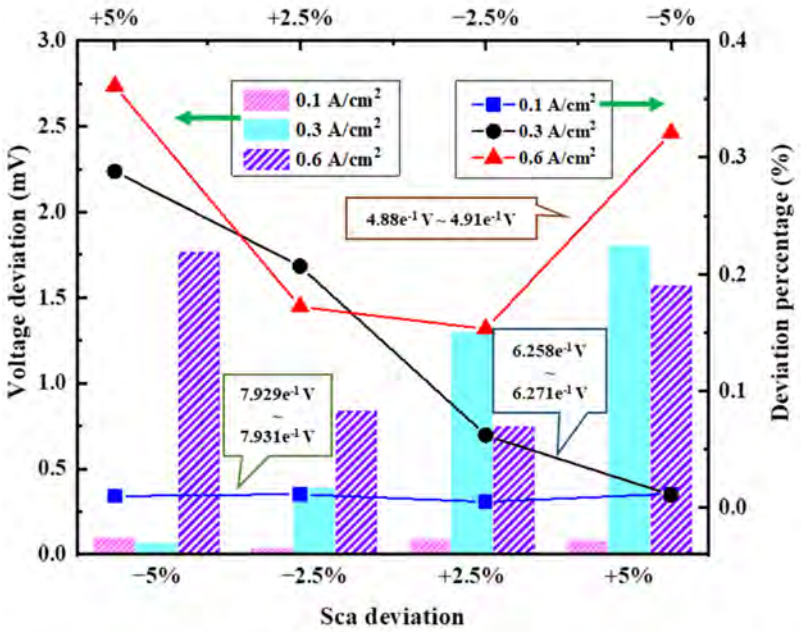

Figure 8. Impacts of CMFR deviations on the voltage deviations and their corresponding percentages under three current densities.

3.3.6. Deviation of Anode/Cathode Inlet Temperature

The effect of deviations of AIT and CIT on the output voltage deviation and deviation percentage are shown in Figures 9 and 10, respectively. Both the AIT and CIT are negatively correlated with the output performance of the fuel cell, which means that at the same current density, the output voltage of the cell increases (decreases) with a decrease (increase) in the anode/cathode intake temperature.

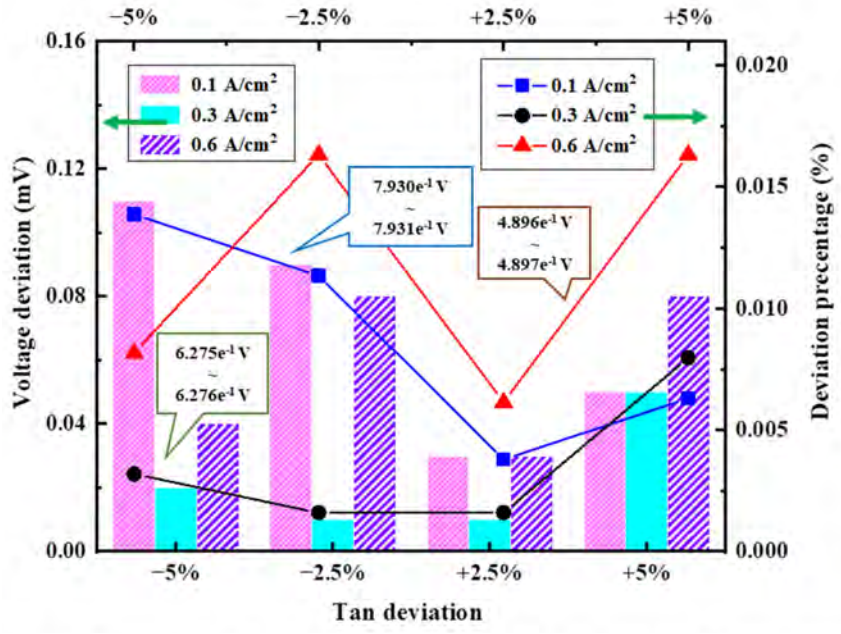

Figure 9. Impacts of AIT deviations on the voltage deviations and their corresponding percentages under three current densities.

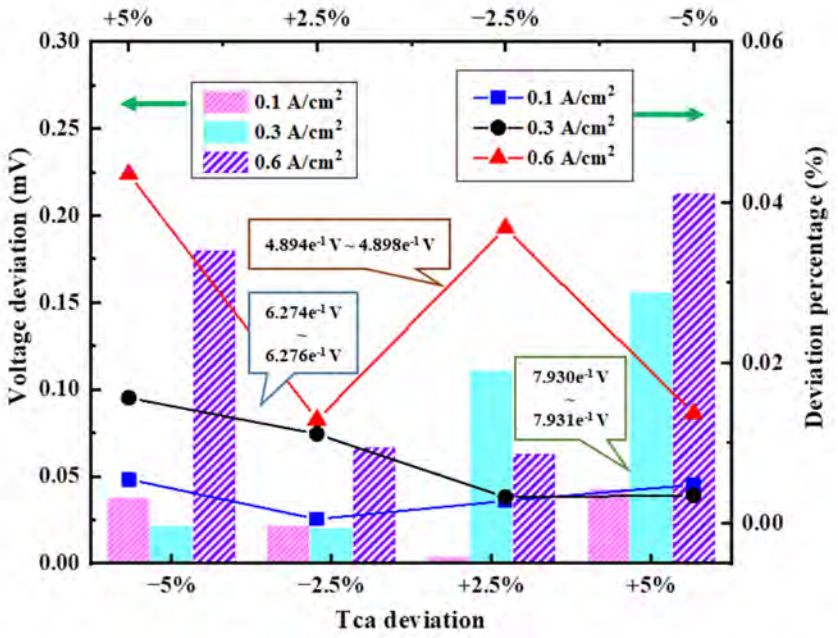

Figure 10. Impacts of CIT deviations on the voltage deviations and their corresponding percentages under three current densities.

The temperature of the reactants can affect the performance of the fuel cell by affecting the relative humidity of the inlet gas. According to the literature [42], the higher inlet temperature corresponds to higher water saturation vapor pressure, the change in absolute humidity is ignored, and the relative humidity of the inlet gas decreases, which ultimately leads to a decrease in PEMFC performance. It can be seen that the larger effect of the AIT deviation on the PEMFC performance, when the current density is 0.1 A/cm^2 from Figures 9 and 10, is because, compared with the cathode, the anode is drier and requires humidification.

3.4. Sensitivity Analysis

3.4.1. Process of Sensitivity Analysis

Above contents discuss how the operating parameters of PEMFC within a certain range of positive and negative deviations impact the deviation of the output voltage and the percentage deviation. According to the pictures of polarization curves and parameter deviations present in Section 3.3, a comparison of the sensitivity of the operating parameters has been obtained. However, there is a nuance of the parameters' sensitivity rankings among the insensitivity indexes.

To further quantify the impact of fluctuation on the insensitive working parameters on the output voltage of the fuel cell under various working current densities, based on the Monte Carlo method, multiparameter sensitivity analysis (MSA) is used to obtain the insensitivity indexes of the output voltage caused by the operating conditions under various current densities. The process of MSA can be expressed as:

(1) Determining the insensitive parameters: T_{an}, T_{ca}, S_{an}, S_{ca} , as seen in Table 4, and defining the deviation range of the standard value as ±5%.
(2) Randomly generating 12 sets of uniform operating parameter values within the range of positive and negative deviation of each parameter, then bringing in the calculated model and obtaining the voltage, which corresponds to the current density as 0.1 A/cm^2, 0.3 A/cm^2, 0.6 A/cm^2, respectively.
(3) Substituting the output voltage from step 2) into the function. Finally, the sensitivity of static evaluation parameters was obtained from Equation (19).

$$f(i) = \sum_{n=1}^{4} [X_{n0}(i) - X_{nc}(i)]^2$$
$$K(i) = k \times \frac{f(i)}{[n \times X_0(i)^2]} \quad (19)$$

(4) where $f(i)$, $K(i)$, $X_0(i)$, and $X_c(i)$ represent the sum of the output voltage deviation, the parameter sensitivities, the reference voltage, and calculated voltage, respectively, when the current density is i. k is the zoom factor and n refers to the number of simulation times when the current density is i.

3.4.2. Results of Analysis

According to the calculation of Equation (19), under different current densities, the sensitivity indexes obtained by four operating parameters within a certain range of deviation (±5%) are depicted in Figure 11. Under the current density that represents the three types of vehicle operating conditions, the sensitivity index of the output voltage was measured. The insensitivity indexes of the operating parameters were observed to be highly nonlinear under various working conditions.

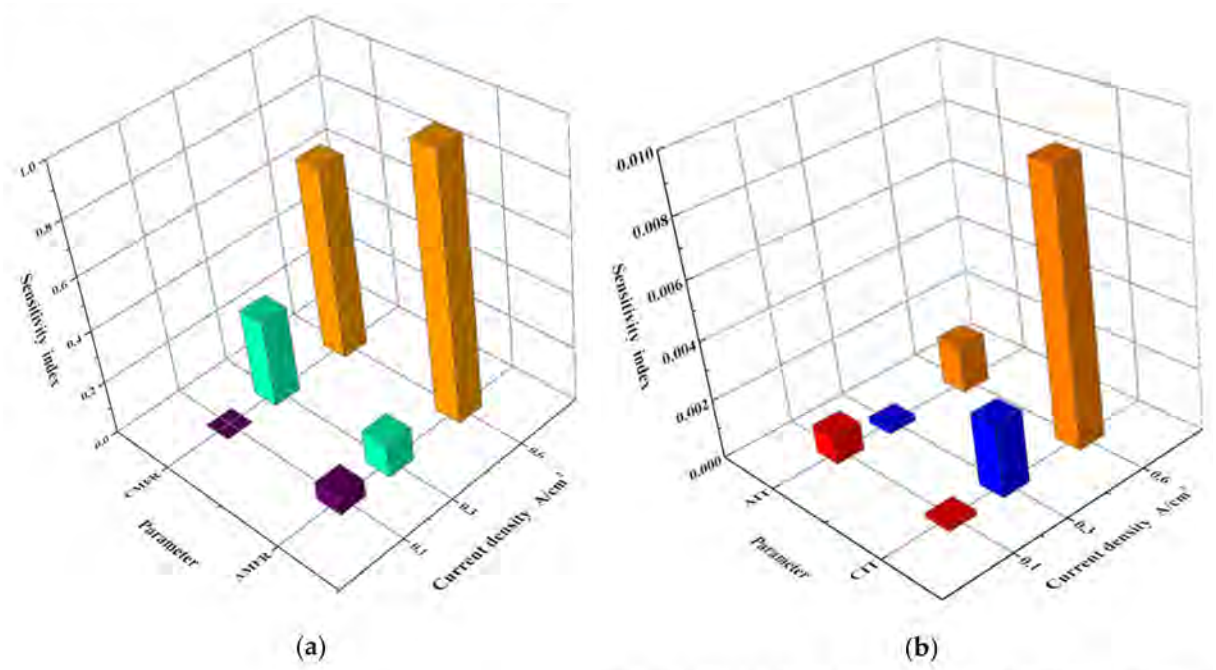

Figure 11. Sensitivity indexes of part of parameters under different current densities: (**a**) Sensitivity indexes comparison between CMFR and AMFR, (**b**) Sensitivity indexes comparison between AIT and CIT.

Among all the parameters, the working temperature of the fuel cell T_{cell} is the most sensitive under three types of conditions (e.g., idle condition, intermediate condition, rated condition). Quantity differences of *y*-axis between Figures 4b and 5b show that the sensitivity index of cathode pressure P_{ca} is far more than the sensitivity index of anode pressure P_{an}. Moreover, with the increase in current density, both the sensitivity indexes of P_{ca} and Pan improve. Even for these insensitive parameters (S_{an}, S_{ca}, T_{an}, and T_{ca}), according to the z-axes of Figure 11a,b, the differences among these sensitivity indexes can be far more than 100 times. By comprehensive comparisons with Figures 3–10, it can be observed that the working parameters tend to have higher sensitivity when the PEMFC is in rated condition.

According to the sensitivity indexes, the parameter sensitivities under various conditions can be ranked as Table 6.

Table 6. Parameter sensitivity rankings.

Operating Conditions	Rankings
Idle condition	$T_{cell} > P_{ca} > P_{an} > S_{an} > S_{ca} > T_{an} > T_{ca}$
Intermediate condition	$T_{cell} > P_{ca} > P_{an} > S_{ca} > S_{an} > T_{ca} > T_{an}$
Rated condition	$T_{cell} > P_{ca} > P_{an} > S_{an} > S_{ca} > T_{ca} > T_{an}$

The parameters are sorted into three groups, which are: very sensitive T_{cell}; normal sensitive P_{ca}, P_{an}; insensitive T_{ca}, T_{an}, S_{ca}, S_{an}.

3.5. Cloud Maps Analysis

The sensitivities of operating parameters of PEMFC are evaluated by digitized form in previous contents. Some sensitive parameters: T_{cell}, P_{ca}, P_{an}, which are evaluated in Section 3.4.2, are used to obtained cloud maps in this section. The effect of fluctuations of these three parameters on performance of PEMFC can reflect on the cloud map, which represents the water content distribution on the interface between membrane and anode CL. Analyzing these cloud maps can more directly explain the fluctuation of operating parameters about how to influence the PEMFC performance.

Due to the too long fuel cell body, only the same part of different cloud maps is intercepted to compare. It can be seen from Figure 12, as the cell temperature decreases, the water content in the interface between the membrane and anode-side CL continues to increase and the water distribution tends to be even. The water content of interfaces increases with the increase of inlet pressure, both in Figures 13 and 14. During the reaction process of PEMFC, water flows from the anode side to cathode side under the impact of electroosmotic migration, which causes the lack of water on the anode side of PEMFC. There is a sharp drop of PEMFC performance when the water content on the anode side is too low; only when the drying effect of the anode side is alleviated can the performance be improved. Moreover, under the fluctuation of the very sensitive parameter T_{cell}, there is the largest difference in the water content distribution on the anode side. The cloud map of water content distribution becomes more and more similar under the fluctuation of parameters with lower sensitivity index. The cloud maps of water content distribution in Figures 12–14 can correspond to the polarization curves of Figures 3–5.

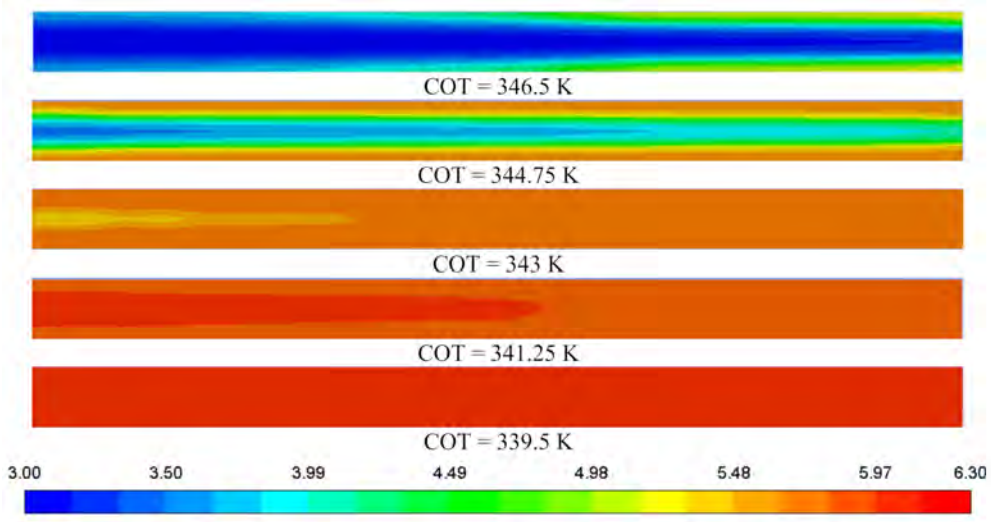

Figure 12. Water content distribution under the fluctuation of COT.

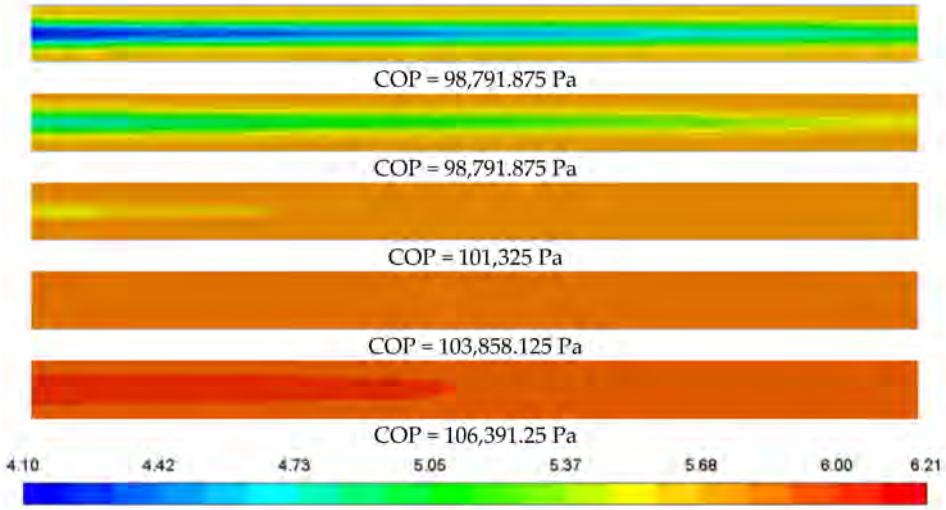

Figure 13. Water content distribution under the fluctuation of COP.

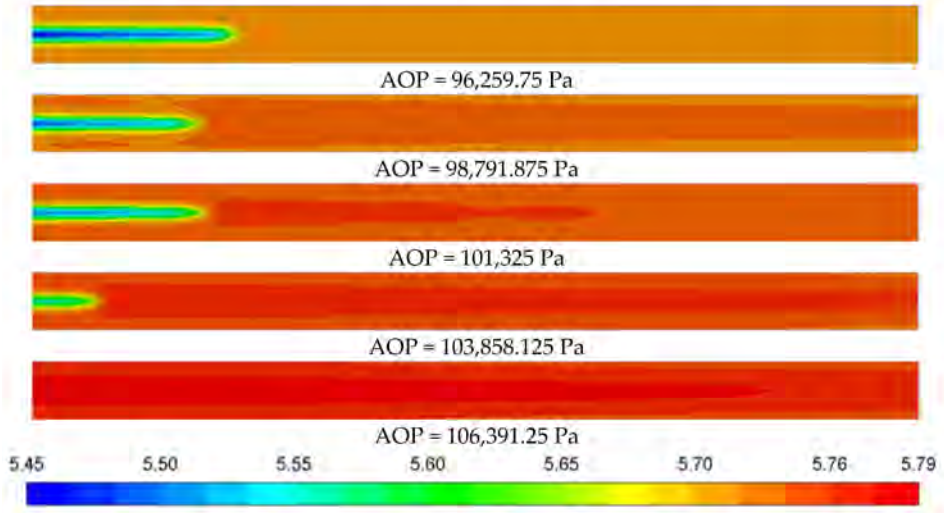

Figure 14. Water content distribution under the fluctuation of AOP.

4. Conclusions

A set of unified parameter fluctuation ranges and evaluation methods, which were combined with the actual operating conditions of PEMFC, has been constructed in this study to avoid the evaluation errors caused by inconsistent standards and to make the results meaningful. The simulation was conducted in a 3D, non-isothemal PEMFC model. Furthermore, a multiparameter sensitivity analysis method combined with the Monte Carlo method was used to evaluate the sensitivity of the working parameter fluctuations ($\pm$5%) to the output performance. Among these parameters, the temperature of the cell is the most sensitive under all working conditions and the sensitivity far exceeds other parameters. However, within the range of deviation, the inlet temperature in both the anode and the cathode has a minimal impact on the output voltage. Moreover, with the increase in current density, the sensitivity indexes of the working pressures in both the anode and the cathode increase, whereas those of the mass flow rate of the anode/cathode change disorderly. Generally, the cathode parameters are more sensitive than the anode parameters, especially under high current density. These results provide a reference for the performance optimization of the PEMFC and a control strategy for the operational parameters.

In future studies, the interaction between the parameters will be considered in order to analyze a more complete working process of the PEMFC.

Author Contributions: Conceptualization, M.P.; Investigation, M.P.; Methodology, J.L.; Project administration, Q.W.; Resources, Q.W.; Software, C.P.; Validation, C.P.; Visualization, C.L. and R.H.; Writing—original draft, C.P. All authors have read and agreed to the published version of the manuscript.

Funding: This research was funded by the Guangxi Key Laboratory of Electrochemical Energy Materials, grant number 7-259-05S002.

Institutional Review Board Statement: Not applicable.

Informed Consent Statement: Not applicable.

Data Availability Statement: Not applicable.

Conflicts of Interest: The authors declare no conflict of interest.

Nomenclature and Abbreviation

List of Symbols

C_p	Specific heat capacity of mixture
D	Diffusion coefficient of gas
D_c	Capillary diffusion coefficient of liquid water
D_m	Diffusion coefficient of water molecules
D_p	Pressure transfer coefficient
F	Faraday constant
j	Exchange current density per unit area (A/cm^2)
P_c	Capillary pressure (bar)
R_{an}	Anode current density (A/cm^2)
R_{ca}	Cathode current density (A/cm^2)
V_{oc}	Open circuit voltage (V)

Source Term

S_m	Source term of mass conservation control equation
S_u	Source term of momentum equation
S_T	Source term of energy equation
S_i	Source term of components conservation
S_l	Source term of transfer current

Greek Symbols

ε	porosity
μ_{eff}	Effective dynamic viscosity
η_{an}	Overpotential of anode surface
η_{ca}	Overpotential of cathode surface
σ_i	Proton membrane conductivity (S/cm)
λ_{eff}	Effective thermal conductivity
ξ	Activation area ratio (1/m)
ϕ_i	Membrane phase voltage (V)
ϕ_{ele}^{an}	Potential on the end plate surface of anode bipolar plates (V)
ϕ_{ele}^{ca}	Potential on the end plate surface of cathode bipolar plates (V)
α_{Rd}^{an}	Anode charge transfer coefficient of reduction reaction
α_{Rd}^{ca}	Cathode charge transfer coefficient of reduction reaction
α_{Ox}^{ca}	Cathode charge transfer coefficient of oxidation reaction
α_{Ox}^{an}	Anode charge transfer coefficient of oxidation reaction
ρ_g	Gaseous water density
ρ_i	Liquid water density

Abbreviation

COT	Cell operating temperature
AIT	Anode inlet temperature
CIT	Cathode inlet temperature
AMFR	Anode mass flow rate
CMFR	Cathode mass flow rate
AOP	Anode operating pressure
COP	Cathode operating pressure

References

1. Shahgaldi, S.; Alaefour, I.; Zhao, J.; Li, X. Impact of ionomer in the catalyst layers on proton exchange membrane fuel cell performance under different reactant flows and pressures. *Fuel* **2018**, *227*, 35–41. [CrossRef]
2. Truc, N.T.; Ito, S.; Fushinobu, K. Numerical and experimental investigation on the reactant gas crossover in a PEM fuel cell. *Int. J. Heat Mass Tran.* **2018**, *127*, 447–456. [CrossRef]
3. Meidanshahi, V.; Karimi, G. Dynamic modeling, optimization and control of power density in a PEM fuel cell. *Appl. Energ.* **2012**, *93*, 98–105. [CrossRef]
4. Jiao, K.; Li, X. Water transport in polymer electrolyte membrane fuel cells. *Prog. Energy Combust. Sci.* **2011**, *37*, 221–291. [CrossRef]
5. Alaswad, A.; Omran, A.; Sodre, J.; Wilberforce Awotwe, T.; Pignatelli, G.; Dassisti, M.; Baroutaji, A.; Olabi, A.G. Technical and Commercial Challenges of Proton-Exchange Membrane (PEM) Fuel Cells. *Energies* **2020**, *14*, 144. [CrossRef]
6. Movahedi, M.; Ramiar, A.; Ranjber, A.A. 3D numerical investigation of clamping pressure effect on the performance of Proton Exchange Membrane fuel cell with interdigitated flow field. *Energy* **2018**, *142*, 617–632. [CrossRef]
7. Zhang, Q.; Xu, L.; Li, J.; Ouyang, M. Performance prediction of proton exchange membrane fuel cell engine thermal management system using 1D and 3D integrating numerical simulation. *Int. J. Hydrogen Energ.* **2018**, *43*, 1736–1748. [CrossRef]
8. Yang, Z.; Du, Q.; Jia, Z.; Yang, C.; Jiao, K. Effects of operating conditions on water and heat management by a transient multi-dimensional PEMFC system model. *Energy* **2019**, *183*, 462–476. [CrossRef]
9. Mohammedi, A.; Sahli, Y.; Moussa, H.B. 3D investigation of the channel cross-section configuration effect on the power delivered by PEMFCs with straight channels. *Fuel* **2020**, *263*, 116713. [CrossRef]
10. Zhao, J.; Shahgaldi, S.; Alaefour, I.; Yang, S.; Li, X. Pore structure and effective diffusion coefficient of catalyzed electrodes in polymer electrolyte membrane fuel cells. *Int. J. Hydrogen Energ.* **2018**, *43*, 3776–3785. [CrossRef]
11. Zhao, J.; Li, X. Oxygen transport in polymer electrolyte membrane fuel cells based on measured electrode pore structure and mass transport properties. *Energ. Convers. Manag.* **2019**, *186*, 570–585. [CrossRef]
12. Qin, Y.; Du, Q.; Fan, M.; Chang, Y.; Yin, Y. Study on the operating pressure effect on the performance of a proton exchange membrane fuel cell power system. *Energ. Convers. Manag.* **2017**, *142*, 357–365. [CrossRef]
13. Kim, J.; Kim, M.; Kang, T.; Sohn, Y.; Song, T.; Choi, K.H. Degradation modeling and operational optimization for improving the lifetime of high-temperature PEM (proton exchange membrane) fuel cells. *Energy* **2014**, *66*, 41–49. [CrossRef]
14. Zhang, Q.; Lin, R.; Técher, L.; Cui, X. Experimental study of variable operating parameters effects on overall PEMFC performance and spatial performance distribution. *Energy* **2016**, *115*, 550–560. [CrossRef]
15. Chavan, S.; Talange, D. Modeling and Performance Evaluation of PEM Fuel Cell by Controlling its Input Parameters. *Energy* **2017**, *138*, 437–445. [CrossRef]
16. Yan, W.; Chen, C.; Mei, S.; Soong, C.; Chen, F. Effects of operating conditions on cell performance of PEM fuel cells with conventional or interdigitated flow field. *J. Power Sources* **2006**, *162*, 1157–1164. [CrossRef]
17. Abdin, Z.; Webb, C.J.; Gray, E.M. PEM fuel cell model and simulation in Matlab–Simulink based on physical parameters. *Energy* **2016**, *116*, 1131–1144. [CrossRef]
18. Wu, H.; Shih, G.; Chen, Y. Effect of operational parameters on transport and performance of a PEM fuel cell with the best protrusive gas diffusion layer arrangement. *Appl. Energ.* **2018**, *220*, 47–58. [CrossRef]
19. Belkhiri, Z.; Zeroual, M.; Ben Moussa, H.; Zereg, M.; Zitouni, B. Numerical simulation of exchange membrane fuel cells in different operating conditions. *Int. J. Hydrogen Energ.* **2012**, *37*, 5444–5451. [CrossRef]
20. Ghasabehi, M.; Ashrafi, M.; Shams, M. Performance analysis of an innovative parallel flow field design of proton exchange membrane fuel cells using multiphysics simulation. *Fuel* **2021**, *285*, 119194. [CrossRef]
21. Hu, M.; Zhao, R.; Pan, R.; Cao, G. Disclosure of the internal transport phenomena in an air-cooled proton exchange membrane fuel cell— part II: Parameter sensitivity analysis. *Int. J. Hydrogen. Energ.* **2021**, *46*, 18589–18603. [CrossRef]
22. Kamal, R.; Chan, S.H. Sensitivity analysis of anode overpotential during start-up process of a high temperature proton exchange membrane fuel cell. *Electrochim. Acta* **2015**, *176*, 965–975. [CrossRef]
23. Zhou, D.; Trang Nguyen, T.; Breaz, E.; Zhao, D.; Clénet, S.; Gao, F. Global parameters sensitivity analysis and development of a two-dimensional real-time model of proton-exchange-membrane fuel cells. *Energ. Convers. Manag.* **2018**, *162*, 276–292. [CrossRef]
24. Vetter, R.; Schumacher, J.O. Experimental parameter uncertainty in proton exchange membrane fuel cell modeling. Part II: Sensitivity analysis and importance ranking. *J. Power Sources* **2019**, *439*, 126529. [CrossRef]
25. Jin, L.; Wang, X.; Zhu, J.; Wang, C.; Zhou, T.; Zhang, X. Sensitivity analysis of proton exchange membrane fuel cell performance to operating parameters and its applicability assessment under different conditions. *Energ. Convers. Manag.* **2021**, *228*, 113727. [CrossRef]
26. Goshtasbi, A.; Chen, J.; Waldecker, J.; Hirano, S.; Ersal, T. Effective Parameterization of PEM Fuel Cell Models—Part I: Sensitivity Analysis and Parameter Identifiability. *J. Electrochem. Soc.* **2020**, *167*, 044504. [CrossRef]
27. Kannan, V.; Xue, H.; Raman, K.; Chen, J.; Fisher, A.; Birgersson, E. Quantifying operating uncertainties of a PEMFC—Monte Carlo-machine learning based approach. *Renew Energ.* **2020**, *158*, 343–359. [CrossRef]
28. Wang, X.; Xu, J.; Lee, D. Parameter sensitivity examination for a complete three-dimensional, two-phase, non-isothermal model of polymer electrolyte membrane fuel cell. *Int. J. Hydrogen Energ.* **2012**, *37*, 15766–15777. [CrossRef]
29. Min, C.H.; He, Y.L.; Liu, X.L.; Yin, B.H.; Jiang, W.; Tao, W.Q. Parameter sensitivity examination and discussion of PEM fuel cell simulation model validation. *J. Power Sources* **2006**, *160*, 374–385. [CrossRef]

30. Elsawwaf, M.; Willems, P.; Feyen, J. Assessment of the sensitivity and prediction uncertainty of evaporation models applied to Nasser Lake. *Egypt. J. Hydrol.* **2010**, *395*, 10–22. [CrossRef]
31. Sobol, I.M. Global sensitivity indices for nonlinear mathematical models and their Monte Carlo estimates. *Math. Comput. Simulat.* **2001**, *55*, 271–280. [CrossRef]
32. Zhao, D.; Dou, M.; Zhou, D.; Gao, F. Study of the modeling parameter effects on the polarization characteristics of the PEM fuel cell. *Int. J. Hydrogen Energ.* **2016**, *41*, 22316–22327. [CrossRef]
33. Chen, H.; Liu, B.; Zhang, T.; Pei, P. Influencing sensitivities of critical operating parameters on PEMFC output performance and gas distribution quality under different electrical load conditions. *Appl. Energ.* **2019**, *255*, 113849. [CrossRef]
34. Oldham, K.; Myland, J. *Fundamentals of Electrochemical Science*; Elsevier: Amsterdam, The Netherlands, 2012.
35. Dickinson, E.J.; Hinds, G. The Butler-Volmer equation for polymer electrolyte membrane fuel cell (PEMFC) electrode kinetics: A critical discussion. *J. Electrochem. Soc.* **2019**, *166*, F221. [CrossRef]
36. Ko, D.; Doh, S.; Park, H.S.; Kim, M.H. Investigation of the effect of operating pressure on the performance of proton exchange membrane fuel cell: In the aspect of water distribution. *Renew Energy.* **2018**, *115*, 896–907. [CrossRef]
37. Zhan, Z.; Zhao, H.; Sui, P.C.; Jiang, P.; Pan, M.; Djilali, N. Numerical analysis of ice-induced stresses in the membrane electrode assembly of a PEM fuel cell under sub-freezing operating conditions. *Int. J. Hydrogen Energ.* **2018**, *43*, 4563–4582. [CrossRef]
38. Husar, A.; Higier, A.; Liu, H. In situ measurements of water transfer due to different mechanisms in a proton exchange membrane fuel cell. *J. Power Sources* **2008**, *183*, 240–246. [CrossRef]
39. Heidary, H.; Kermani, M.J.; Dabir, B. Influences of bipolar plate channel blockages on PEM fuel cell performances. *Energ. Convers. Manag.* **2016**, *124*, 51–60. [CrossRef]
40. Hayre, R.; Cha, S.; Colella, W.; Prinz, F.B. *Fuel Cell Fundamentals*; John Wiley & Sons: New York, NY, USA, 2016.
41. Ogungbemi, E.; Wilberforce, T.; Ijaodola, O.; Thompson, J.; Olabi, A.G. Review of operating condition, design parameters and material properties for proton exchange membrane fuel cells. *Int. J. Energ. Res.* **2021**, *45*, 1227–1245. [CrossRef]
42. Barbir, F. *PEM Fuel Cells: Theory and Practice*; Academic Press: New York, NY, USA, 2012.